Modern Control Theory for Design of Autopilots for Bank-to-Turn Missiles

Douglas E. Williams* and Bernard Friedland†
The Singer Company, Kearfott Division, Little Falls, New Jersey
and
Appasaheb N. Madiwale‡
MIT Lincoln Laboratories, Lexington, Massachusetts

The state-space techniques of modern control theory are used to develop a methodology for the design of autopilots for bank-to-turn missiles. The methodology accommodates the gyroscopic and coriolis cross-coupling between the pitch and the yaw axes that result from the high roll rates that may be present. The design assumes that the roll rate is constant but not zero, and it results in an autopilot structure in which there are cross-couplings between the pitch and yaw channels that are dependent on the roll rate. The autopilot gains are also scheduled as functions of the dynamic pressure. A reduced-order extended Kalman filter with fixed gains is used to estimate the actuator states and the commanded acceleration. The performance of an autopilot designed by this methodology was evaluated in a six-degree-of-freedom simulation using the dynamics of a typical high-performance tactical missile. Excellent performance in terms of low miss distance and small sideslip is obtained.

Introduction

TWO basic methods of controlling the attitude of a missile to achieve the acceleration commanded by the guidance law are skid-to-turn (STT) and bank-to-turn (BTT). In the former, the roll angle may be either held constant or uncontrolled; in either case, the magnitude and orientation of the body acceleration vector is achieved by permitting the missile to develop both an angle of attack and a sideslip angle. The presence of the sideslip imparts a "skidding" motion to the missile; hence the name "skid-to-turn." A bank-to-turn missile, on the other hand, should ideally not have any sideslip. To achieve the desired orientation of the missile, it is rolled (banked) so that the plane of maximum aerodynamic normal force is oriented to the desired direction and the magnitude of the force is controlled by adjusting the attitude (angle of attack) in that plane.

The design of an autopilot for a highly maneuverable bank-to-turn missile poses a severe challenge to the designer. High maneuverability means not only high aerodynamic accelerations but also the ability to change the orientation of the acceleration rapidly. This means that the roll rates can be expected to be much larger (perhaps by an order of magnitude) than they would be in a skid-to-turn missile, which reorients the aerodynamic acceleration by changing the ratio of the angle of attack to the angle of sideslip. The large roll rates induce substantial coriolis and gyroscopic cross-coupling between the pitch and the yaw axes, while in a typical skid-to-turn missile this cross-coupling is negligible. To reckon with the effects of cross-coupling requires the designer to consider both axes together as a single multiple-input/multiple-output system. The problem is further complicated by the fact that the cross-axes couplings are proportional to the roll rate, which is a dynamic variable. This means that the dynamics of the pitch and yaw axes are not only cross-coupled but also nonlinear.

One method of treating the cross-axes couplings in a BTT missile is to treat them as unknown disturbances (which, in effect, is to ignore them) and to design controllers for the pitch and the yaw axes independently, but with good disturbance rejection properties, so that the transient cross-axis disturbances do not seriously affect the system performance. This appears to be the design approach used by Emmert et al.[1] in their dither-adaptive bank-to-turn autopilot design. Another approach, studied by Arrow,[2] begins with an uncoupled single-axis design for each channel. A coordination branch is then added which couples the yaw to the roll channel in an attempt to counteract the pitch into yaw coriolis cross-coupling effects. Both these approaches appear to give adequate performance for small roll rates.

If a control system could be designed to cope with high roll rates, however, the response time to out-of-plane acceleration commands would be reduced and the performance of the missile, particularly against evasive targets, would be improved. The objective of our design approach is to exploit the potential reduction in response time by explicitly accounting for the cross-axis couplings and treating the coupled pitch and yaw axes together as a single system.

The dynamic model of the missile, especially when the actual dynamics are included, is complicated enough to require the use of computer-aided design methods. At the present time such methods are limited to linear systems. Thus, as a practical matter, we must stick to linear models. To accomplish this for the nonlinear missile dynamics, we make an assumption that we call the "adiabatic approximation." This assumes that the roll rate changes slowly enough to be treated as a constant for each design point. For each fixed roll rate, a steady-state control law is determined with the aid of suitable software, using the linear, quadratic, Gaussian (LQG) design methodology. The control law is then implemented by scheduling the resulting gains as functions of the roll rate. The control gains are also scheduled as functions of the dynamic pressure. This means that each of the pitch/yaw gains (of which there are twenty) can be a function of two variables. It may seem that this would result in a horrendous implementation problem, but this does not appear to be the case. Each of the gains is adequately represented by a fairly simple analytical expression, the coefficients of which are determined by the computer-aided de-

Received March 31, 1986; revision received Nov. 12, 1986.

*Scientist.

†Manager, Systems Research. Associate Fellow AIAA.

‡Staff Member.

sign software. The implementation in a modern airborne digital computer is, if anything, less complicated than a more conventionally designed autopilot.

The autopilot structure that results from this approximation is shown in Fig. 1. The inputs are the pitch- and yaw-commanded accelerations that are generated by the guidance computation, the sensed body rates p, q, and r, and two components of the normal components of specific force which are called "vertical" and "lateral" acceleration. The dynamics are formulated so that the sensed quantities are state variables, so the sensor outputs are used directly as inputs to the control law gains. In addition to the state variables that are measured directly, however, there are other state variables (namely the actuator states) that we assume are not measurable. (In most cases, it would be possible to instrument the measurement of the actuator states, if the control law required them, but a conventionally designed autopilot does not require these inputs and it may not be convenient to bring them into the flight control computer.) A reduced-order[3] Kalman filter is thus employed to estimate the unmeasurable states. To provide some "integral" control action, the commanded accelerations are also regarded as state variables to be estimated.

As Fig. 1 shows, there are twenty control ("regulator") gains, each of which can be scheduled as a function of dynamic pressure and roll rate. The variation with respect to roll rate, however, is confined primarily to ten of the gains in which the variation with the roll rate is approximately linear. These are identified as cross-feed gains, which are shown as proportional to the roll rate. It is these cross-feed gains that arise only when the coriolis and gyroscopic moments are considered in the dynamics that impart the outstanding performance to the system.

Missile Dynamic Model

For purposes of design, the missile dynamics are represented by the following set of differential equations:

Pitch:

$$\dot{e}_z = \frac{Z_\alpha}{V} e_z + Z_\alpha q + Z_{\delta q}\dot{\delta}_q + \frac{Z_\alpha}{V} a_{zc} - \left\{\frac{Z_\alpha}{Y_\beta} e_y - \frac{Z_\alpha Y_\delta}{Y_\beta}\delta_r + \frac{Z_\alpha}{Y_\beta} a_{yc}\right\} p$$

$$\dot{q} = \frac{M_\alpha}{Z_\alpha} e_z + M_q q + \left(M_{\delta q} - \frac{Z_{\delta q} M_\alpha}{Z_\alpha}\right)\dot{\delta}_q + \frac{M_\alpha}{Z_\alpha} a_{zc} + \left\{\frac{I_{zz} - I_{xx}}{I_{yy}} r\right\} p$$

$$\ddot{\delta}_q = \omega^2(u_{\delta q} - \delta_q) - 2\zeta\omega\dot{\delta}_q$$

$$\dot{a}_{zc} = 0 \qquad (1)$$

Yaw:

$$\dot{e}_y = \left\{\frac{Y_\beta}{Z_\alpha} e_z - \frac{Y_\beta Z_{\delta q}}{Z_\alpha}\delta_q + \frac{Y_\beta}{Z_\alpha} a_{zc}\right\} p + \frac{Y_\beta}{V} e_y - Y_\beta r + Y_{\delta r}\dot{\delta}_r + \frac{Y_\beta}{V} a_{yc}$$

$$\dot{r} = \left\{\frac{I_{xx} - I_{yy}}{I_{zz}} q\right\} p + \frac{N_\beta}{Y_\beta} e_y + N_r r + \left(N_{\delta r} - \frac{Y_{\delta r} N_\beta}{Y_\beta}\right)\delta_r + \frac{N_\beta}{Y_\beta} a_{yc}$$

$$\ddot{\delta}_r = \omega^2(u_{\delta r} - \delta_r) - 2\zeta\omega\dot{\delta}_r$$

$$\dot{a}_{yc} = 0 \qquad (2)$$

Roll:

$$\dot{e}_\phi = p$$

$$\dot{p} = L_p p + L_{\delta p} u_{\delta p} + L_\beta \beta \qquad (3)$$

where the missile speed is $V = (u^2 + v^2 + w^2)^{1/2}$, u, v, and w are the projections of the vehicle velocity vector on the body x, y, and z axes, respectively, and $u_{\delta q}$, $u_{\delta r}$, and $u_{\delta p}$ are the commanded effective surface deflections in pitch, yaw, and roll, respectively. Also used in the preceding equations and elsewhere are the following definitions:

$\alpha = w/u$ = angle of attack
$\beta = v/u$ = angle of sideslip
$a_z = Z_\alpha \alpha + Z_{\delta q}\delta_q$
$a_y = Y_\beta \beta + Y_{\delta r}\delta_r$
a_{zc} = commanded acceleration along z body axis
a_{yc} = commanded acceleration along y body axis
$e_z = a_z - a_{zc}$ = error in acceleration along z body axis
$e_y = a_y - a_{yc}$ = error in acceleration along y body axis
e_ϕ = error in bank angle
p = roll rate
q = pitch rate
r = yaw rate
δ_q = effective pitch control surface deflection
δ_r = effective yaw control surface deflection

Defining the errors e_z and e_y as state variables is particularly useful since the autopilot is to be designed to minimize these quantities during the flight. Moreover, since accelerometers as well as rate gyros are available for measurements, these error states are directly measurable.

In addition to the error states, the commanded accelerations are also included in the state vector. If the commanded acceleration is assumed to be constant in inertial coordinates, then the differential equations governing these states are

$$\dot{a}_{zc} = 0$$

$$\dot{a}_{yc} = 0$$

The error in the bank angle is defined as

$$e_\phi = \arctan(a_{yc}/a_{zc}) \qquad (4)$$

On taking the time derivative of e_ϕ and calculating the derivatives of the commanded acceleration in body coordinates, the first equation of Eq. (3) is obtained.

Regarding the dynamic model of Eqs. (1–3), it is noted that 1) The aerodynamic stability derivatives Z_α, $Z_{\delta q}$, Y_β, $Y_{\delta r}$, M_α, M_q, $M_{\delta q}$, N_β, N_r, $N_{\delta r}$, L_p, $L_{\delta p}$, and L_β are, in general, complicated functions of many variables including the Mach number, the dynamic pressure Q_0 and, particularly in the case of aerodynamic moments, the variation in the mass, the moments of inertia, and the center of gravity due to the rocket engine mass flow.

2) Significant cross-coupling exists between the pitch dynamics, the yaw dynamics, and the roll dynamics. The cross-coupling in these equations is not only explicit but also implicit (due to the dependence of some aerodynamic terms on cross-axis dynamics). The explicit terms are the result of both coriolis and gyroscopic moments. The coriolis and gyroscopic terms present in Eqs. (1) and (2) are enclosed in braces and multiplied by the roll rate p.

Observe that all explicit cross-coupling is proportional to the roll rate and that consequently these terms vanish when the latter goes to zero. When the roll rate is large, however, these explicit cross-coupling terms can significantly affect the dynamic response of the missile.

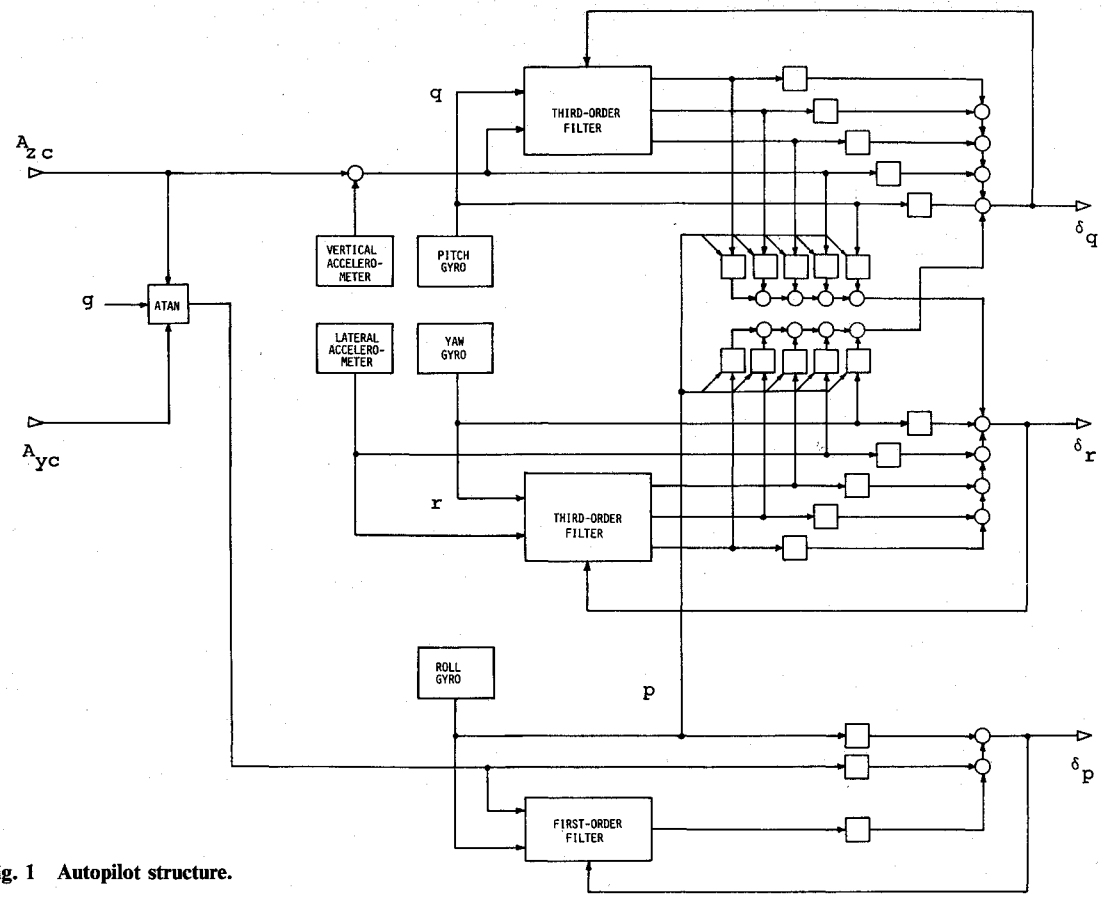

Fig. 1 Autopilot structure.

Design Approach

The function of the autopilot is to cause the achieved acceleration of the missile to match the commanded acceleration as closely as possible, consistent with operating constraints on the missile and control actuators. For a bank-to-turn missile, the most significant constraint is on the allowable sideslip. Ideally, the sideslip should be zero, which would result in completely coordinated turns. This condition cannot be met exactly, but the requirement that the sideslip be kept small motivates the choice of weighting factors in the performance criterion that the autopilot design is intended to minimize. The reasons for minimizing the sideslip in a BTT missile are twofold. If the resulting sideslip angle becomes too large it can, in conjunction with a large angle of attack, produce large rolling moments. These induced rolling moments can be two or even three times larger than the maximum moment required to execute a typical 90-deg roll. As a result, the additional effective roll control surface deflection required (which is generated using the same actuators required for pitch and yaw maneuvers) may cause control saturation, resulting in possible instability or reduced maneuverability. At the very least, these induced roll moments will make accurate control of the bank angle more difficult, which is critical to obtaining high performance in a BTT missile. In addition to the problem of induced rolling moments, if an air-breathing ram-jet type of propulsion system is to be used, the angle of sideslip must be kept small in order to insure the proper operation of this type of engine.

Regulator Design

Owing to the presence of the coriolis and gyroscopic coupling between the pitch and yaw axes, the process dynamics are nonlinear. The problem of the nonlinearity is avoided through the use of the "adiabatic approximation":[4] the dynamics are linearized by assuming that the roll rate is constant at every instant of time. This uncouples the roll axis from the pitch and yaw axes and permits the use of linear, quadratic, Gaussian design methodology with its associated software tools.

Thus, the design equations comprise two linear systems, hereafter referred to as the "pitch/yaw channel" and the "roll channel." As mentioned earlier, the roll channel design is fairly straightforward and is not discussed here for reasons of space. The pitch/yaw channel can be represented in state-space notation by

$$x = [e_z,\ q,\ \delta_q,\ \dot{\delta}_q,\ a_{zc} \mid e_y,\ r,\ \delta_r,\ \dot{\delta}_r,\ a_{yc}]'$$

$$u = [u_{\delta q} \mid u_{\delta r}]' \tag{5}$$

The dynamics can then be expressed in the standard state-space form

$$\dot{x} = Ax + Bu \tag{6}$$

in which A and B are partitioned in conformity with the partitioning of x and u:

$$A = \begin{bmatrix} A_{11} & A_{12} \\ A_{21} & A_{22} \end{bmatrix} \qquad B = \begin{bmatrix} B_1 \\ B_2 \end{bmatrix} \tag{7}$$

The submatrices of A are each 5-x-5 matrices in which A_{21} and A_{12} contain the explicit cross-coupling terms (coriolis and gyroscopic) between the pitch and yaw channels. All nonzero terms in the latter are linear functions of the roll rate (assumed contant).

A typical performance goal for a cruciform wing airframe employing a skid-to-turn control policy might be to track each of the resultant commanded normal accelerations, equal in magnitude to $(a_{zc}^2 + a_{yc}^2)^{1/2}$. This, however, is not a suitable goal for a monowing airframe that must employ a bank-to-

turn (BTT) control policy because the yaw maneuvering capability of the monowing airframe is quite small (less than 5 g for a typical airframe). Actually, even a 5 g steady-state yaw acceleration is often not desirable as it may also be important to keep the sideslip angle as small as possible.

In view of the small yaw maneuvering capability, one cannot hope to achieve any appreciable yaw acceleration while at the same time minimizing the sideslip angle. Thus the performance criterion for the pitch/yaw channel is to track only the pitch component of the commanded acceleration while maintaining a small sideslip angle. A performance criterion that embraces these requirements is of the form

$$J = \int_t^\infty (C_1^2 e_z^2 + C_2^2 e_y^2 + C_3^2 \beta^2 + C_4^2 \delta_q^2 + C_5^2 \delta_r^2 + C_6^2 u_{\delta q}^2 + C_7^2 u_{\delta r}^2)\, d\tau \tag{8}$$

In accordance with the adiabatic approximation, the control law that minimizes this performance criterion is given by

$$u = -Gx$$

in which the gain matrix G is given by

$$G = R^{-1}B'M$$

where M is the solution to the algebraic Riccati equation

$$O = MA + A'M - MBR^{-1}B'M + Q \tag{9}$$

in which the matrices Q and R are the state and control weighting matrices defined implicitly by the performance criterion of Eq. (8). The gain matrix G is a 2-x-10 matrix.

Since the solution to Eq. (9) and the resulting gains will, in general, vary with the particular A and B matrices used, solutions are obtained at many points within the operating envelope. In addition, since A and B vary as a function of many variables (dynamic pressure, Mach number, air density, roll rate, mass and inertia variation due to thrust, etc.), the choice of design points and independent variables that produce gain variations could become prohibitively large even for computer-aided design techniques. Experimentation within the design procedure and knowledge of the underlying physical process is necessary in order to determine which parameter variations must be explicitly accounted for in the resulting design and which can be handled by making the design robust.

From experience we have found that the only explicit parameter variations that need to be considered are the roll rate p and the dynamic pressure Q_0. A roll rate variation from -8 to 8 rad/s and a dynamic pressure variation from 1000 to 9000 lb/ft^2 (corresponding to a Mach number variation at 10,000 ft of approximately 1.0 to 3.0) were used. The gain matrices for each of approximately 40 design points are computed using numerically reliable software. The resulting gains are then fit using a least squares curve fitting routine to a number of different functional models with the roll rate and dynamic pressure as the independent variables. The resulting curve fits are then examined by the designer, who selects one model for each gain on the basis of a tradeoff between analytical complexity and goodness of fit.

Our experience has also been that the gains from the pitch axis states to the pitch surface deflection command and from the yaw axis states to the yaw axis surface deflection command are nearly independent of roll rate and linear in dynamic pressure. The cross-axis gains, i.e., the gains from the pitch axis states to the yaw surface deflection command and vice versa, are essentially independent of dynamic pressure and linear in roll rate.

The weighting factors in the performance integral Eq. (8) are constant for all point designs within the operating envelope. Our viewpoint is that Eq. (8) is considered to be a good approximation of the true performance objectives and should therefore be equally valid at all operating conditions. But as a result, the closed loop poles vary significantly with dynamic pressure and roll rate. This is in direct contrast to other design techniques that attempt to provide nearly constant dynamic response over the entire operating envelope. The former approach offers the opportunity of providing much faster system response at high dynamic pressure where aerodynamic control is enhanced. This can be a significant advantage, especially in scenarios with maneuvering targets. Conversely, at low dynamic pressure the response time is increased. This in turn may help reduce control saturation.

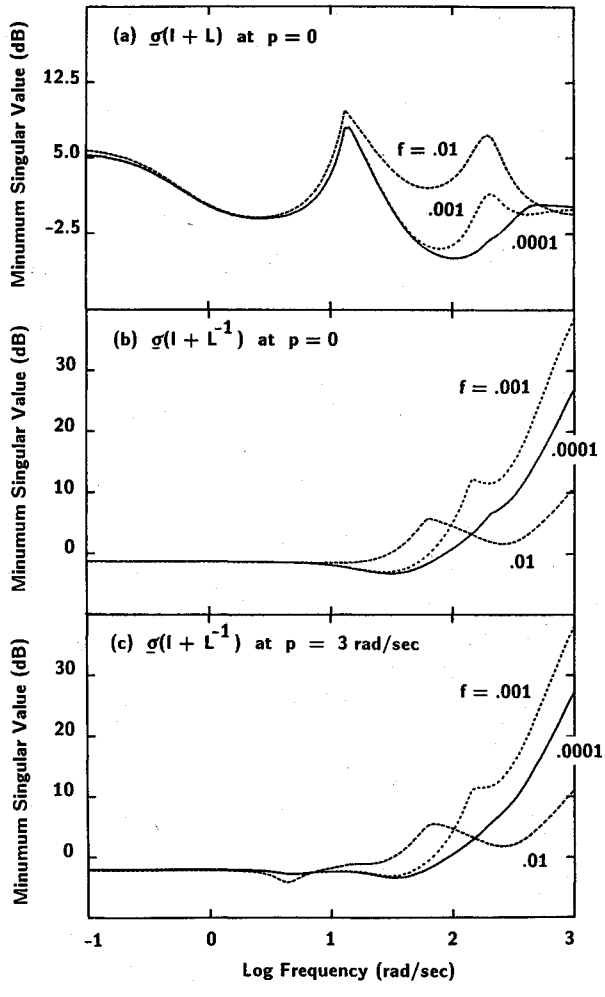

Fig. 2 Singular value plots of pitch/yaw channel return difference for loop opened at control surface inputs.

The roll channel is treated as a single-input/single-output subsystem, the gains of which are designed by pole placement. Three gains are required for the roll channel.

In summary, counting the gains of the roll channel, the autopilot controller design requires 23 gains, all of which are scheduled as functions of dynamic pressure. In addition, 20 gains are also scheduled as functions of the roll rate p. The resultant scheduling functions (involving at most products of dynamic pressure and roll rate) are fairly simple, and thus the computational burden of gain scheduling is not excessive.

Reduced-Order Observers

In accordance with the separation principle, an observer is designed to obtain the required estimates of the states used in the control laws for the pitch/yaw channel and for the roll channel. The structure in both designs is that of a reduced-order observer. This choice is made primarily in an effort to simplify the resulting compensator to the maximum extent justified. The sensors (three rate gyros and three accelerome-

ters) are assumed to be of high enough quality to permit the resulting measurements to be considered essentially noise-free. As a result, the required estimates of those states directly measured by the sensors are assumed to be the sensor outputs themselves. The order of the required dynamic observers is thus reduced to the number of state variables that cannot be directly measured. As in the regulator design, the "adiabatic approximation" is used to linearize the dynamics and to separate the pitch/yaw channel from the roll channel.

Pitch/Yaw Channel

The observer for the pitch/yaw channel is designed as a reduced-order Kalman filter. The state vector is

$$\bar{x} = [\bar{x}_1' \mid \bar{x}_2']' \tag{10}$$

where

$$\bar{x}_1 = [e_z, q, e_y, r]'$$

$$\bar{x}_2 = [\delta_q, \dot{\delta}_q, a_{zc}, \delta_r, \dot{\delta}_r, a_{yc}]'$$

Note that $\bar{x}_1$ and $\bar{x}_2$ together contain the same state variables as appear in Eq. (5), but that the partitioning into $\bar{x}_1$ and $\bar{x}_2$ is on the basis of states that are measured or not measured, respectively, rather than on pitch or yaw. The states in $\bar{x}_1$ are directly measurable while those in $\bar{x}_2$ are not. Consequently the observation equation is

$$y = \bar{x}_1 = C\bar{x} \tag{11}$$

with

$$C = [I, 0]$$

where I is a 4-x-4 identity matrix and 0 is a 4-x-6 null matrix.

The process dynamics for which the observer is to be designed are of the form

$$\dot{\bar{x}} = \bar{A}\bar{x} + \bar{B}u + \bar{F}v \tag{12}$$

The elements of the dynamics matrix $\bar{A}$ and control matrix $\bar{B}$ in Eq. (12) are the same as those in Eq. (6), but arranged in a different order to reflect the partitioning Eq. (10); v is a vector of white noise sources and $\bar{F}$ is the process noise distribution matrix. These matrices may be partitioned as follows:

$$\bar{A} = \begin{bmatrix} \bar{A}_{11} & \bar{A}_{12} \\ 0 & \bar{A}_{22} \end{bmatrix} \qquad \bar{B} = \begin{bmatrix} 0 \\ \bar{B}_2 \end{bmatrix} \qquad \bar{F} = \begin{bmatrix} F_1 \\ F_2 \end{bmatrix}$$

As shown in Ref. 3, a reduced-order observer for this model, assuming noise-free observations, is given by

$$\hat{x}_1 = y$$

$$\hat{x}_2 = Hy + z \tag{13}$$

where z is an auxiliary dynamic variable given by

$$\dot{z} = A_{\text{obs}}z + G_{\text{obs}}y + \bar{B}_2u \tag{14}$$

$$A_{\text{obs}} = \bar{A}_{22} - H\bar{A}_{12}$$

$$G_{\text{obs}} = A_{\text{obs}}H - H\bar{A}_{11}$$

The matrix H appearing in the preceding equations is the gain matrix of the reduced-order Kalman filter given by Ref. 3:

$$H = (P\bar{A}_{12}' + F_2\bar{V}F_1')(F_1\bar{V}F_1')^{-1} \tag{15}$$

Here $\bar{V}$ is the 8-x-8 process noise spectral density matrix of the white noise input vector v and P is the 6-x-6 steady-state covariance matrix obtained by the solution of the steady-state reduced-order variance equation

$$0 = \tilde{A}P + P\tilde{A}' - P\bar{A}_{12}'(F_1\bar{V}F_1')^{-1}\bar{A}_{12}P + \tilde{V} \tag{16}$$

where

$$\tilde{A} = \bar{A}_{22} - F_2\bar{V}F_1'(F_1\bar{V}F_1')^{-1}\bar{A}_{12}$$

$$\tilde{V} = F_2\bar{V}F_2' - F_2\bar{V}F_1'(F_1\bar{V}F_1')^{-1}F_1\bar{V}F_2'$$

All the matrices except the noise distribution submatrices F_1 and F_2, and the process noise spectral density matrix $\bar{V}$ are specified by the assumed open-loop dynamics at the particular design condition of interest. By choosing these matrices the designer can influence the resulting dynamics of the pitch/yaw channel observer.

For this design, the 8-x-8 matrix $\bar{V}$ is diagonal, specifying eight independent white noise sources. These eight noise sources enter the dynamic Eqs. (12) in a specific way through the noise distribution submatrices F_1 and F_2 in order to provide the desired pitch/yaw observer dynamics. Notice in Eq. (16) that $\tilde{A}$ and $\tilde{V}$ require the existence of $(F_1\bar{V}F_1')^{-1}$ in order to be defined. The existence of $(F_1\bar{V}F_1')^{-1}$ is equivalent to requiring that four of the eight noise sources be distributed in a linearly independent way to the dynamics associated with the four states measured by the sensors, i.e., e_z, q, e_y, and r. A physical interpretation can be given to these noise sources by assuming that they model the unknown and/or variable aerodynamics that produce unknown forces and moments acting on the vehicle. Similarly, two other noise sources are used to model the uncertain commanded acceleration time histories a_{zc} and a_{yc}. Finally, two independent noise sources are added at the control inputs $u_{\delta q}$ and $u_{\delta r}$. These noise sources are distributed to the dynamics equations in exactly the same manner as the control inputs themselves. These last two noise sources are chosen and distributed in this particular way in order to enhance the robustness of the resulting compensator, as will be discussed in the next section.

It was anticipated that the resulting pitch/yaw observer gain matrix H would be scheduled as a function of either roll rate and/or dynamic pressure in order to provide accurate state estimates for use in the pitch/yaw control law. We have found, however, in a number of simulations that good performance can be achieved using a constant H matrix obtained at a zero roll rate, low dynamic pressure design point. Thus the twenty-four elements of the gain matrix H are implemented as constants. This result represents a major simplification in the overall compensator structure.

Roll Channel

A roll channel observer is designed using the pole placement technique to estimate the unmodeled aerodynamic disturbance term $L_\beta\beta$ that is denoted here as an exogenous input $D(\alpha, \beta)$, which is modeled as an unknown constant. As in the pitch/yaw design, a reduced-order observer is used. The choice of this form as in the pitch/yaw design is based on the assumption that the measurement uncertainties are very small compared to the uncertainty in the process itself.

The reduced-order roll observer is given by

$$\hat{x}_1 = y$$

$$\hat{x}_2 = Hy + z \tag{17}$$

$$\dot{z} = F\hat{x}_2 + G_{\text{obs}}y + Eu_{\delta p}$$

The same symbols are used for the roll observer as were used in Eq. (14) for the pitch/yaw observer. In this channel, however, the observation vector y comprises the error in the roll angle e_ϕ and the roll rate p. The roll angle error is obtained using the known guidance law outputs a_{zc} and a_{yc}. The roll rate is obtained from the output of the roll rate gyro. The other

matrices are given by

$$H = [h_1, h_2] \qquad F = -H\bar{A}_{12}$$
$$G_{obs} = -H\bar{A}_{11} \qquad E = -H\bar{B}$$

where $\bar{A}_{11}$ etc. correspond to the following partioning of the state vector:

$$\bar{x}_1 = [e_\phi, p] \qquad \bar{x}_2 = D(\alpha, \beta)$$

This partitioning results in

$$\bar{A} = \begin{bmatrix} \bar{A}_{11} & \bar{A}_{12} \\ 0 & 0 \end{bmatrix}$$
$$\bar{B} = \begin{bmatrix} 0 \\ L_{\delta p} \end{bmatrix}$$

The choice of the gain matrix H, together with the assumed open-loop dynamics, completely determines the roll channel observer. For this particular implementation, h_1 is chosen to satisfy the relation

$$h_1 = -h_2 L_p$$

This choice makes $G_{obs} = 0$, although the state estimate $\hat{x}_2$ still depends on y. The second gain h_2 is chosen to produce a sufficiently high speed of response in order to provide adequate estimation of the disturbance $D(\alpha, \beta)$. The gain matrices for the design obtained by the use of this design technique, accompanied by representative aerodynamic characteristics, are given in Appendix A.

Robustness Analysis

The mathematical model of the missile dynamics used in the design of this autopilot may differ from the actual missile dynamics due to variation in aerodynamics, linearization, unmodeled cross-axis coupling, and high-frequency dynamics, etc. The parameters of the mathematical model are obtained from wind tunnel tests, which are subject to experimental errors. In addition, errors exist due to autopilot simplifications such as gain scheduling and constant gain observer. Hence an autopilot designed based on the mathematical model has to perform satisfactorily in the presence of various errors and maintain missile stability.

In this study, we use the Doyle–Stein[5] procedure for the robustness recovery of LQG-based autopilot designs. In this procedure, fictitious process noise is assumed present at inputs, and its variance is increased until satisfactory robustness is obtained. To evaluate the robustness of the resulting designs, we use singular-value analysis and guaranteed gain and phase margins derived from the singular values.[6-9]

In our approach to BTT autopilot design, the reduced-order observer is designed based on Eq. (12). But the first two columns of $\bar{F}$ are nothing but the matrix $\bar{B}$. Hence we can rewrite Eq. (12) as

$$\dot{\bar{x}} = \bar{A}\bar{x} + \bar{B}u + f\bar{B}v_1 + F^* v_2 \qquad (18)$$

where in Eq. (12) $\bar{F} = [\bar{B}, F^*]$ and $v = [fv_1, v_2]'$ and f is a scalar parameter that can be varied to increase or decrease the fictitious process noise at the input.

It can be shown that the loop transfer function with loop open at the input is

$$L = L_2 L_1$$

where the open-loop aerodynamic transfer function is

$$L_1 = C(sI - \bar{A})^{-1}\bar{B}$$

and the compensator transfer function is

$$L_2 = (G_1 + G_2 H) + G_2(sI - A_{obs} + \bar{B}_2 G_2)^{-1}(G_{obs} - \bar{B}_2[G_1 + G_2 H])$$

The matrices G_1 and G_2 represent the partitioning of the pitch/yaw regulator gain matrix according to the measured and estimated states, respectively.

The multivariable gain and phase margins are based on the singular values of $I + L$ and $I + L^{-1}$ developed by Lehtomaki et al.[7] It is well known that stability margins obtained using singular-value analysis are very conservative.[8] Safonov[9] has shown that the use of Peron eigenvalues may generally result in less conservative bounds on diagonal perturbation. In this study, margins are computed using both the singular values and the Peron eigenvalues, and the least conservative margins are obtained by the union of the three sets of margins.

Robustness enhancement of the BTT autopilot design frozen at Mach 1.38 and dynamic pressure $Q_0 = 2000$ lb/ft^2 is carried out using five values of the scalar parameter f in Eq. (18). The robustness was evaluated using the singular-value plots and multivariable gain and phase margins. The frequency range used is from 0.1 to 1000 rad/s, which was extended to 10,000 rad/s in some cases. The scalar was varied from 0.0001 to 1.0. The robustness was enhanced with the roll rate frozen at zero and then evaluated at roll rates 0 and 3 rad/s.

Case 1: Roll Rate = 0

The minimum singular values of $I + L$ are shown in Fig. 2a for $f = 0.0001$, 0.001, and 0.01. There is very little change in the singular value in the frequency range of 0.1 to 10 rad/s. The increase in f resulted in larger minimum singular value and hence better robustness in the midfrequency range of 10 to 500 rad/s. The robustness at a higher frequency range is best illustrated by the minimum singular value plot of $I + L^{-1}$ shown in Fig. 2b. The minimum singular value of the design with $f = 0.001$ is larger than that with $f = 0.001$ or 0.01 in the frequency range of 100 to 1000 rad/s. Thus, increasing f beyond 0.001 results in a reduction in robustness at higher frequencies and little improvement at middle frequencies.

The gain and phase margins for the preceding designs were computed and are presented in Table 1. These margins increase monotonically as f is increased from 0.001 to 1.0. For large values of f of 0.1 and 1.0, the robustness margins are essentially recovered. Although larger gain and phase margins are obtained with larger f, the resulting observers have poles with very large negative real parts. These are undesirable owing to implementation and noise rejection considerations. As noted previously, there is a reduction in robustness at higher frequencies at larger values of f. Hence we selected the design with $f = 0.001$ with more than adequate gain margins $[-10.8, 8.7]$ and phase margins of ± 41.6 deg.

Case 2: Roll Rate = 3 rad/s

The minimum singular values of $I + L^{-1}$ are shown in Fig. 2c. The minimum singular value for the design with $f = 0.01$ is smaller than other two designs at frequency 4.6 rad/s, and hence it is less robust. The reason is that we are using a subop-

Table 1 Least conservative gain and phase margins at zero roll rate

	Gain margins, dB		
f	Reduction	Increase	Phase margins, deg
0.0001	−10.2	7.3	±40.4
0.001	−10.8	8.7	±41.6
0.01	−16.0	19.9	±53.4
0.1	−18.4	38.2	±59.2
1.0	−18.0	57.2	±59.9

timal simplified reduced-order observer with a constant gain matrix that was designed at zero roll rate. The high-frequency behavior is similar to the results for designs with zero roll rate.

The multivariable gain and phase margins for a 3 rad/s roll rate in Table 2 do not increase monotonically with increasing f. There is a sudden decrease in margins for $f = 1$. This again is due to the suboptimal observer used. To confirm this, the margins were computed at a 3 rad/s roll rate with an optimal observer, and we found that the margins increased monotonically with increasing f. However, the margins for suboptimal design were better than the optimal design at lower values of f. This is another reason for our selection of the design with $f = 0.001$.

It is noted that this method enhances robustness only at the input, where the loop is assumed to be broken for the singular-value analysis. Robustness with regard to the variation of parameters at other points in the system is not necessarily enhanced. This limitation became apparent when we found that relatively small errors (of the order of 10%) in the feedback gain matrix, which resulted from the use of curve-fit expressions for gain scheduling, could produce large changes in the closed-loop response—in extreme cases, even instability. We found that the problem could be alleviated by increasing the weighting in the performance integral Eq. (8) on those states having gains that were found to be especially sensitive to parameter variation.

Performance Evaluation

In order to assess the performance characteristics of the autopilot design in a closed-loop air-to-air intercept scenario, it is necessary to specify, in addition to the control law, the target dynamics and the guidance law. For the simulation results presented here, the target dynamics are given by an algorithm developed by Riggs and Vergez.[10] This algorithm models the target as a point mass. The target initially travels at constant velocity; then two-step changes in acceleration, each of 9 g magnitude, occur. The first step occurs when the range to the target reaches 6000 ft, and the second occurs when the time-to-go drops to less than 1 s. The directions of these accelerations are constrained to be normal to the target velocity and to have a component normal to the encounter plane. Thus the missile acceleration vector must be reoriented after launch to achieve an interception.

The following guidance law was selected:

$$A_c = K(R_r + V_r t_{go})/t_{go}^2 \tag{19}$$

where A_c denotes the three-component vector of commanded accelerations, R_r denotes the three-component vector of relative position, V_r denotes the three components of the relative velocity vector, t_{go} is the time-to-go, and K is the navigation constant. The time-to-go is calculated using the formula[10]

$$t_{go} = 2r_x/[-v_x + (v_x^2 + 4r_x a_x/K)^{1/2}] \tag{20}$$

where a_x is the axial missile acceleration and r_x and v_x are the components of the relative position and velocity vectors in the direction of the missile x axis.

By computing the time-to-go in this manner, the component of commanded acceleration along the missile centerline is made equal to the actual missile acceleration in this direction in an attempt to account for the uncontrollable missile thrust. In order to minimize the effects of the guidance error, all the quantities required in Eqs. (19) and (20) are assumed to be known exactly.

In the actual implementation, a "g-bias" is introduced in the autopilot in order to counteract the effects of gravity. This is accomplished by converting the total acceleration command given in Eq. (19) to a specific force acceleration by subtracting the gravity vector. The components of this commanded specific force vector along the z and y body axes are then used to compute the error in the roll angle as defined by Eq. (4). The z component enters the pitch/yaw autopilot unchanged. But since the pitch/yaw channel is designed to match only the pitch components of the commanded acceleration, the yaw component is set to zero.

Table 2 Least conservative gain and phase margins for roll rate = 3 rad/s

	Gain margins, db		
f	Reduction	Increase	Phase margins, deg
0.0001	− 9.9	7.1	±39.8
0.001	−10.6	8.3	±41.2
0.01	− 9.1	9.6	±39.0
0.1	−10.0	13.3	±46.0
1.0	− 8.0	6.0	±34.8

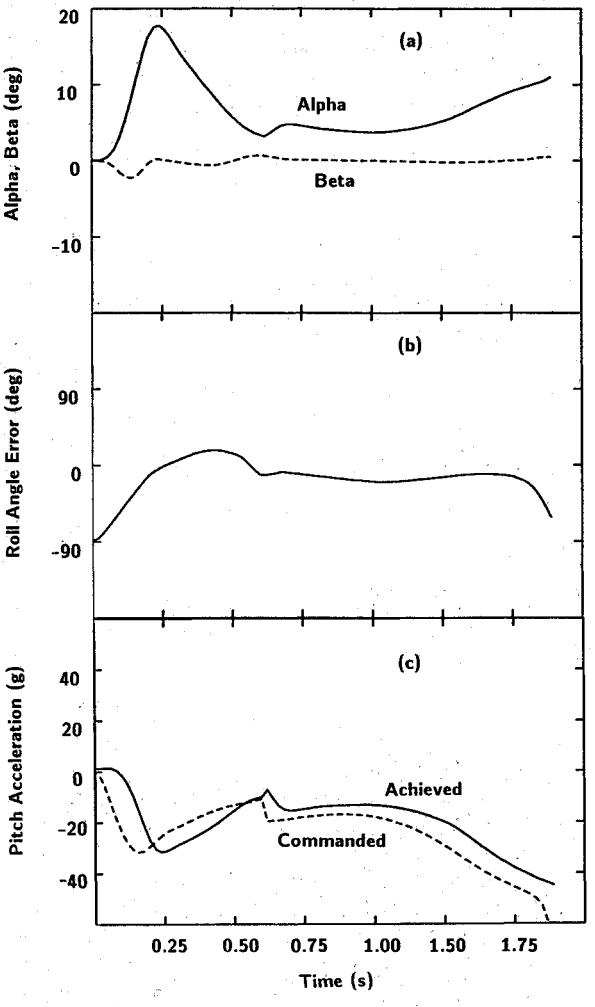

Fig. 3 Intercept time histories at design altitude of 10,000 ft.

The results to be described were obtained with an accurate six-degree-of-freedom simulation in which all the gyroscopic and coriolis couplings were accurately modeled. The aerodynamic parameters were obtained from tabular aerodynamic data via multidimensional linear interpolation routines. Therefore, all implicit aerodynamic cross-couplings are retained. Also, the effect of the missile thrust on mass and inertia variations as well as aerodynamic moment variations due to the displacement of the center of gravity are included.

The performance time histories are presented in Fig. 3 for a moderately difficult interception scenario in which the target is initially 4000 ft downrange of the missile. The initial aspect angle is 135 deg and the initial boresight angle is 0 deg. The

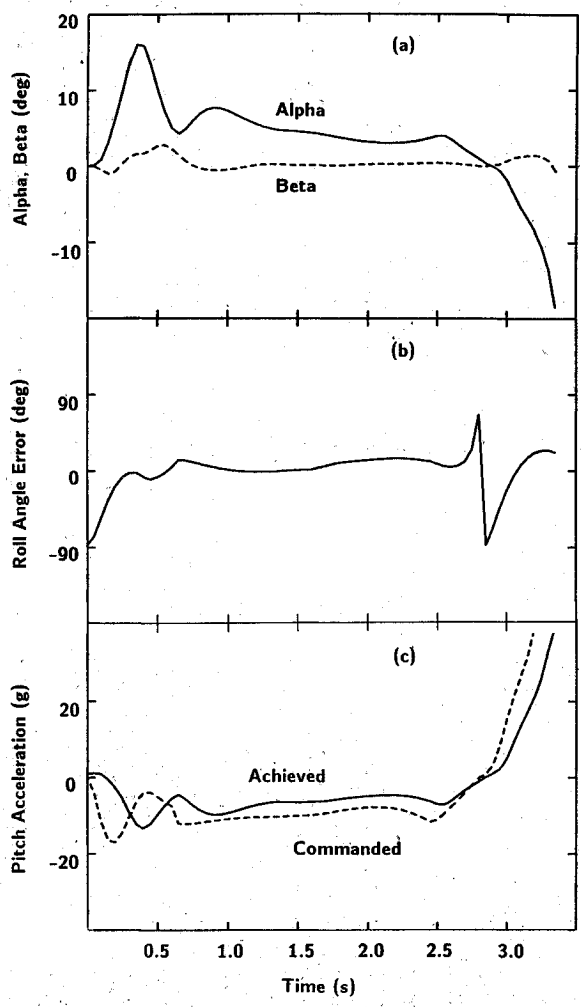

Fig. 4 Interception time histories at altitude of 40,000 ft.

target and missile both have the initial speed of 970 ft/s and the same altitude of 10,000 ft.

Figure 3a gives the time histories of the angle of attack and angle of sideslip. After an initial transient (of a maximum angle of 2.5 deg) the sideslip is below 1 deg. This shows excellent turn coordination even in the presence of large initial disturbances (coriolis and gyroscopic) due to simultaneously large angle of attack and roll rate. Figure 3b shows the roll error. The nonzero error after the initial transient can be attributed to the effect of target maneuvers. Even though the angle error does not go to zero in the steady state, excellent performance is achieved. The miss distance is 2.1 ft.

Figure 3c shows the commanded and achieved total accelerations resolved along the z body axis. These accelerations track each other quite well, although the error does not go to zero as it would if true integral control were present. The step change in the commanded acceleration and the resulting transient occurring at about $t = 0.6$ s in the achieved acceleration are due to a step change in axial acceleration that is caused by a thrust level transition. This transition affects the time-to-go guidance calculation Eq. (20) and consequently results in a step change in the commanded acceleration.

To investigate the ability of this autopilot to function effectively outside of the range of operating conditions for which it was specifically designed, an intercept scenario was simulated with the missile and target in altitude at 40,000 ft. Because the gains were designed for a 10,000-ft altitude, this 40,000-ft altitude scenario required that the resulting gain variations due to dynamic pressure be extrapolated outside the design region to accommodate the lower dynamic pressure. The high-altitude time histories are shown in Fig. 4.

Figure 4a presents the angle of attack and angle of sideslip time histories. Even at this lower dynamic pressure, the turn coordination is still excellent and the maximum sideslip is only slightly larger than that for the previous scenario. Figure 4b shows the roll angle error for this trajectory, which is quite similar to that presented for the lower altitude case. There is a large transient, however, in the last second of the trajectory due to the "last ditch" maneuver of the target. This transient does not appear to degrade the performance, however, as this engagement resulted in a 6.7 ft terminal miss distance.

The commanded and achieved total accelerations in the z body direction show quite good agreement (Fig. 4c). The lag between the commanded and the actual acceleration is greater, however, due to the longer autopilot response times at the reduced dynamic pressure.

The effect of the cross-coupling gains on the resulting autopilot performance was also investigated. A test scenario was generated using the identical conditions as used for the run of Fig. 4, except that all the cross-coupling gains are set to zero. The resulting control law is equivalent to our design for zero roll rate where no explicit cross-coupling is present. It was found that the sideslip angle increased to a maximum of 8 deg and that greater roll angle errors were present. The terminal miss distance was increased to 30 ft. While bank-to-turn autopilots designed without the explicit cross-coupling terms may all not show the same lack of coordination exhibited in the test scenario, these results are representative of the type of difficulties that can be expected when explicit cross-coupling effects are not included in the design equations.

Conclusions

This study has demonstrated the application of a design methodology for autopilots for bank-to-turn missiles based on the state-space techniques of modern control theory. The autopilot design that has emerged from the use of this technique exhibits excellent performance in terms of terminal miss distance and well-coordinated turns over a wide range of operating conditions. In using this design method (as well as any other method), it is necessary to verify satisfactory behavior at all expected operating conditions by analysis and extensive simulation. In this regard, we noted a tendency to yaw axis instability in our design at flight regimes with high Mach number combined with high angle of attack. This, we expect, can be corrected by a change in the weighting factors used in the regulator design.

The choice of suitable weighting factors to achieve the most appropriate tradeoff between performance (miss distance), operation within the constraints of control surface deflection, saturation, etc., and robustness with respect to parameter variations remain open questions. We have developed several rules of thumb for setting the suitable weighting factors for a general class of missiles.

The availability of an integrated set of computer-aided design programs is a significant advantage in permitting the engineer to rapidly investigate the effect of a change in a weighting parameter of the performance of the autopilot. We have applied the design technique to three different missiles of quite different aerodynamic characteristics. In all cases we have been successful in designing an autopilot that meets performance objectives within realistic constraints upon the missile.

The autopilot design described in this paper would doubtless be implemented using an airborne digital computer: either a microprocessor committed to this computation, or a portion of a general guidance and control computer. In either case, the implementation requirements are not excessive by current standards. In an implementation study that we performed using the actual code for the autopilot,[11] we estimated that the autopilot would require about 30% of the available time on a state-of-the-art airborne computer.

Appendix A: Representative Data

Flight Conditions

Altitude	= 10,000 ft
Mach no.	= 1.38
Q_0	= 2000 lb/ft^2
α	= 8 deg
β	= 0 deg

Stability Derivatives

$Z_\alpha = -4571$ ft/s^2	$Y_\beta = -1287$ ft/s^2	$L_p = -2.6$ l/s
$Z_{\delta q} = -1175$ ft/s^2	$Y_{\delta r} = 1207$ ft/s^2	$L_{\delta p} = 11113$ l/s^2
$M_\alpha = 149$ l/s^2	$N_\beta = 295$ l/s^2	$L_\beta = -6438$ l/s^2
$M_{\delta q} = -701$ l/s^2	$N_{\delta r} = -695$ l/s^2	
$M_q = -0.028$ l/s	$N_r = -0.028$ l/s	

Observer Feedback Gain Matrices

$$H = \begin{bmatrix} 0.9E-5 & -0.73E-5 & 0 & 0 \\ -0.11 & 0.1E-5 & 0 & 0 \\ 0 & 0 & -0.14E-5 & -0.58E-5 \\ 0 & 0 & 0.12 & -0.3E-5 \\ -0.998 & -0.078 & 0 & 0 \\ 0 & 0 & -0.54 & -1.7 \end{bmatrix}$$

$$L = [95.4 \quad 60]$$

Control Gains

Pitch/Yaw Channel

Inputs	Outputs: δ_q (pitch)		δ_r (yaw)	
e_z	$4.5E-4$		$(-5.6E-5+7.3E-9*Q_0)$	$*p$
q	$-9.3E-2-1.3E-5*Q_0$		$5.8E-3$	$*p$
δ_q	$0.5 \quad +3.4E-4*Q_0$		$-4.3E-2$	$*p$
δ_q	$5.0E-3+6.0E-7*Q_0$		$-3.3E-5$	$*p$
a_{zc}	$-4.0E-5$		$(-1.4E-5+1.2E-8*Q_0)$	$*p$
e_y	$(3.2E-5-4.6E-9*Q_0)$	$*p$	$7.3E-3+3.8E-7*Q_0$	
r	$6.5E-4$	$*p$	$-0.35 \quad -6.6E-5*Q_0$	
δ_r	$-1.1E-2$	$*p$	$7.22 \quad +2.3E-3$	$*Q_0$
δ_r	$-3.0E-6$	$*p$	$1.1E-2+1.8E-6*Q_0$	
a_{yc}	$(8.9E-6-8.0E-9*Q_0)$	$*p$	$-6.5E-3+9.0E-7*Q_0$	

Roll Channel

$$\delta_R = [25.5e_\phi + 3.3p + 0.21D(\alpha,\beta)]/Q_0$$

Acknowledgment

This investigation was performed for the U.S. Air Force Armament Laboratory under Contract F08635-83-C-0371.

References

[1]Emmert, R. I. et al., "Detailed Stability and Control Investigations of a Bank-to-Turn Configuration," AFATL-TR-78-10, Air Force Armament Laboratory, Eglin AFB, FL, Jan. 1972.

[2]Arrow, A., "An Analysis of Aerodynamic Requirements for Coordinated Bank-to-Turn Autopilots," NASA-CR-3644, Nov. 1983.

[3]Friedland, B., *Control System Design: An Introduction to State-Space Methods*, McGraw-Hill Book Company, New York, NY, 1986.

[4]Friedland, B., Richman, J., and Williams, D. E., "On the 'Adiabatic Approximation' for Design of Control Laws for Linear, Time-Varying Systems," *Proceedings of the American Control Conference*, Seattle, WA, June, 1986, pp. 623–627.

[5]Doyle, J. C. and Stein, G., "Robustness with Observers," *IEEE Transactions on Automatic Control*, Vol. AC-24, Aug. 1979, pp. 607–618.

[6]Safonov, M. G. and Athans, M., "Gain and Phase Margin for Multiloop LQG Regulators," *IEEE Transactions on Automatic Control*, Vol. AC-22, April 1977, pp. 173–179.

[7]Lehtomaki, N. A., Sandell, N. A., and Athans, M., "Robustness Results in LQG Based Multivariable Control Designs," *IEEE Transactions on Automatic Control*, Vol. AC-26, 1981, pp. 75–91.

[8]Barrett, M. F., "Conservatism with Robustness Tests for Linear Feedback Control Systems," *Proceedings of the IEEE Conference on Decision and Control*, Albuquerque, NM, Dec. 1980, pp. 885–890.

[9]Safonov, M. G., "Stability Margins of Diagonally Perturbed Multivariable Feedback Systems," *Proceedings of the IEEE Conference on Decision and Control*, San Diego, CA, Dec. 1981, pp. 1472–1478.

[10]Riggs, T. L. and Verges, P. L., "Advanced Air-to-Air Guidance Using Optimal Control and Estimation," AFATL-TR-81-56, Air Force Armament Laboratory, Eglin AFB, FL, June 1981.

[11]Williams, D. E., Madiwale, A. N., and Friedland, B., "Modern Control Theory for Autopilots," AFATL-TR-85-10, Air Force Armament Laboratory, Eglin AFB, FL, June 1985.